Eur. Phys. J. A (2013) **49**: 65
DOI 10.1140/epja/i2013-13065-0

THE EUROPEAN PHYSICAL JOURNAL A

Regular Article – Experimental Physics

Measurements of $^{12}C(\vec{\gamma}, pp)$ photon asymmetries for $E_\gamma = 200$–450 MeV

The Crystal Ball at MAMI and A2 Collaborations

J. Robinson[1], I.J.D. MacGregor[1,a], J.R.M. Annand[1], P. Aguar-Bartolomé[2], L.K. Akasoy[2], H.J. Arends[2], Ya.I. Azimov[3], K. Bantawa[4], R. Beck[5], V.S. Bekrenev[3], H. Berghäuser[6], A. Braghieri[7], D. Branford[8], W.J. Briscoe[9], J. Brudvik[10], S. Cherepnya[11], R.F.B. Codling[1], B.T. Demissie[9], M. Dieterle[12], E.J. Downie[2], P. Drexler[2], L.V. Fil'kov[11], D.I. Glazier[8], R. Gregor[6], D. Hamilton[1], E. Heid[2], D. Hornidge[13], D. Howdle[1], O. Jahn[2], T.C. Jude[8], V.L. Kashevarov[11], I. Keshelashvili[12], R. Kondratiev[14], M. Korolija[15], M. Kotulla[6], A.A. Koulbardis[3], S.P. Kruglov[3], B. Krusche[12], V. Lisin[14], K. Livingston[1], D.M. Manley[4], J.C. McGeorge[1], E.F. McNicoll[1], V. Metag[6], D.G. Middleton[2,13], A. Mushkarenkov[7], B.M.K. Nefkens[10], A. Nikolaev[5], R. Novotny[6], M. Oberle[12], M. Ostrick[2], R.O. Owens[1], P.B. Otte[2], B. Oussena[2], P. Pedroni[7], A. Polonski[14], S. Prakhov[10], G. Rosner[1], T. Rostomyan[7], S. Schumann[2], M.H. Sikora[8], D.I. Sober[16], A. Starostin[10], I.I. Strakovsky[9], I.M. Suarez[10], I. Supek[15], C.M. Tarbert[8], M. Thiel[6], A. Thomas[2], M. Unverzagt[2], D.P. Watts[8], D. Werthmueller[12], and L. Witthauer[12]

[1] SUPA, School of Physics and Astronomy, University of Glasgow, Glasgow G12 8QQ, UK
[2] Institut für Kernphysik, University of Mainz, D-55099 Mainz, Germany
[3] Petersburg Nuclear Physics Institute, 188300 Gatchina, Russia
[4] Kent State University, Kent, Ohio 44242, USA
[5] Helmholtz-Institut für Strahlen- und Kernphysik, University of Bonn, D-53115 Bonn, Germany
[6] II Physikalisches Institut, University of Giessen, D-35392 Giessen, Germany
[7] INFN Sezione di Pavia, I-27100 Pavia, Italy
[8] SUPA, School of Physics, University of Edinburgh, Edinburgh EH9 3JZ, UK
[9] The George Washington University, Washington, DC 20052, USA
[10] University of California Los Angeles, Los Angeles, California 90095-1547, USA
[11] Lebedev Physical Institute, 119991 Moscow, Russia
[12] Institut für Physik, University of Basel, CH-4056 Basel, Switzerland
[13] Mount Allison University, Sackville, New Brunswick E4L3B5, Canada
[14] Institute for Nuclear Research, 125047 Moscow, Russia
[15] Rudjer Boskovic Institute, HR-10000 Zagreb, Croatia
[16] The Catholic University of America, Washington, DC 20064, USA

Received: 2 April 2013 / Revised: 9 May 2013
Published online: 30 May 2013

Communicated by P. Rossi

Abstract. The $^{12}C(\vec{\gamma}, pp)$ reaction has been studied in the photon energy range 200–450 MeV at the Mainz microtron MAMI-C, where linearly polarised photons were energy-tagged using the Glasgow-Mainz Tagged Photon Spectrometer and protons were detected in the Crystal Ball detector. The photon asymmetry Σ has been measured over a wider E_γ range than previous measurements. The strongest asymmetries were found at low missing energies where direct emission of nucleon pairs is expected. Cuts on the difference in azimuthal angles of the two ejected protons increased the magnitude of the observed asymmetries. At low missing energies the Σ data exhibit a strong angular dependence, similar to deuteron photodisintegration.

1 Introduction

Two-nucleon knockout reactions from light nuclei using real or virtual photons at energies of a few hundred MeV proceed by mechanisms that involve Meson Exchange Currents (MEC), Isobar Currents (IC), Short-Range Correlations (SRC) and Final-State Interactions (FSI) [1–3]. The reaction amplitudes are also dependent on the final state of the residual nucleus. To clarify the contributions from each of these processes it is necessary to make measurements with both real and virtual photons over a wide range of kinematic conditions and to study both proton-neutron and proton-proton emission.

[a] e-mail: douglas.macgregor@glasgow.ac.uk

In recent years polarised photons have provided access to observables sensitive to the details of the reaction process, whose effects are hidden when averaged over the total response. Cross sections for reactions in which the polarisation of the incident photon is either parallel ($\sigma_\parallel$) or perpendicular ($\sigma_\perp$) to the plane of the emitted protons have different sensitivity to the reaction mechanisms that contribute. This difference is emphasised through the photon asymmetry, $\Sigma = \frac{\sigma_\parallel - \sigma_\perp}{\sigma_\parallel + \sigma_\perp}$. Polarised photon measurements therefore provide a powerful tool to study details of two-nucleon emission reactions and to test models of the reaction process.

This paper reports measurements of the ^{12}C($\vec{\gamma}$,pp) reaction made with linearly polarised photons in the energy range $E_\gamma = 200$–450 MeV. The near 4π angular coverage of the Crystal Ball (CB) detector, used to detect protons, allowed investigation of the photon asymmetry Σ over a wide range of proton angles.

2 Photonuclear reaction models

An understanding of which specific mechanisms contribute to (γ,NN) reactions at different missing energies has been obtained from the Valencia model [4] which uses a microscopic treatment of photon-nucleus coupling at intermediate energies including pion FSI. The model includes multi-pion and multi-nucleon production processes in complex nuclei. Pion production processes, including resonant and non-resonant terms, account for the propagation and interaction of the Δ in the nuclear medium. It treats the nucleons statistically using a Fermi gas approach, related to real nuclei by a local density approximation. The products of the initial interaction are tracked through the nuclear medium using a semi-classical approach to account for any further interactions in the nuclear medium.

Despite its approximations, the Valencia model gives a good account of the shape and strength of the ^{12}C(γ,pn) missing energy spectrum and the shape of the ^{12}C(γ,pp) spectrum [5], suggesting that the relative contributions from different processes and FSI are reasonably well described. These studies indicated that for the mechanism to be predominantly two-body, a restriction has to be made to the low energy part of the residual excitation spectrum. At high missing energies E_m much of the two-nucleon knockout strength appears to be fed by initial pion production followed by FSI.

More detailed descriptions of two-nucleon knockout reactions require treatments of nuclear wave functions. The most detailed calculations have been made by the Gent [3, 6, 7] and Pavia [1, 8, 9] groups with models of proton-neutron and proton-proton emission that use an unfactorised treatment and include the effects of FSI.

Calculations by the Gent group [3] investigated ^{12}C in quasideuteron kinematics, in which the recoil momentum $\mathbf{P}_r$ is zero. For ^{12}C(γ,pp), calculations of emission from $(1p_{3/2})^2$ orbits for $E_\gamma = 100$–400 MeV showed that coupling to 0^+ final states was much stronger than to 2^+ states. The calculations showed that isobar currents dominated the asymmetry even at low E_γ and that the effects of using an unfactorised treatment and distorted outgoing nucleon waves were very important.

3 Previous measurements with polarised photons

Only a few two-nucleon knockout measurements with polarised photons have been reported for nuclei heavier than deuterium. Measurements of Σ for ^{3}He($\vec{\gamma}$,pp) and ($\vec{\gamma}$,pn) have been carried out at LEGS [10] for $E_\gamma = 235$–305 MeV. These measurements showed strong differences between ($\vec{\gamma}$,pp) and ($\vec{\gamma}$,pn) reactions. Calculations, which are in reasonably good agreement with the experimental measurements, indicated one- and two-body terms dominate ($\vec{\gamma}$,pn) while three-body terms dominate ($\vec{\gamma}$,pp).

Further Σ measurements for ^{6}Li($\vec{\gamma}$,pn) and ^{4}He($\vec{\gamma}$,pn) have been made at the 3.5 GeV Yerevan electron synchrotron [11], although these data were averaged over a wide range of E_m.

More detailed measurements of ^{12}C($\vec{\gamma}$,pn) and ($\vec{\gamma}$,pp) were carried out in quasideuteron kinematics using the PiPToF detector arrays in Mainz [12, 13]. Missing energy cuts $E_\mathrm{m} < 40$ MeV and $E_\mathrm{m} = 40$–70 MeV were applied to select event samples dominated by emission from $(1p)^2$ and (1p)(1s) orbitals, respectively. The data were analysed in three photon energy regions: $E_\gamma = 160$–220 MeV, $E_\gamma = 220$–280 MeV and $E_\gamma = 290$–350 MeV. In both reaction channels Σ was negative in all photon energy regions. $\Sigma_{(\gamma,\mathrm{pp})}$ showed a strong negative peak whose magnitude exceeded $\Sigma_{(\gamma,\mathrm{pn})}$ at low E_m. This was interpreted as showing that (γ,pp) is dominated by a direct knockout mechanism at low E_m. At higher E_m, Σ has lower magnitude and the differences between the two channels become small. Unpolarised photon experiments on ^{12}C [14–17, 5], and comparisons with Valencia model predictions, indicate mechanisms involving intermediate pion production dominate both channels at high E_m, with little strength from direct 2N emission. This may offer an explanation for the similarity and small magnitude of Σ observed in the two reaction channels.

A very limited investigation of the angular distribution of ^{12}C($\vec{\gamma}$,pp) and ^{12}C($\vec{\gamma}$,pn) has been carried out [18]. The statistical accuracy was too poor to allow the angular dependence of Σ to be determined. However, measurements of the differential cross sections with the reaction plane parallel ($\sigma_\parallel$) or perpendicular ($\sigma_\perp$) to the polarisation plane were made for ToF polar angles from 47° to 76°. For ($\vec{\gamma}$,pp), significant differences were observed between the angular distributions of $\sigma_\parallel$ and $\sigma_\perp$. For $E_\mathrm{m} < 40$ MeV, $\sigma_\perp$ is larger than $\sigma_\parallel$, with the largest observed differences at smaller ToF angles for $E_\gamma = 160$–220 MeV, and at larger ToF angles for $E_\gamma = 290$–350 MeV. For $40 < E_\mathrm{m} < 70$ MeV significant differences between $\sigma_\parallel$ and $\sigma_\perp$ are only apparent for the highest E_γ range. The strong observed energy and angular dependences of $\sigma_\parallel$ and $\sigma_\perp$ indicate that Σ is likely to be very sensitive to the contributing reaction mechanisms.

4 Experiment

A beam of electrons from the Mainz Microtron (MAMI-C) [19,20] was directed onto a 100 μm thick diamond radiator and produced linearly polarised photons, which were energy-tagged using the Glasgow-Mainz Tagged Photon Spectrometer [21–23]. The tagged photons were tightly collimated before hitting a carbon target positioned in the centre of the Crystal Ball detector [24]. A Particle Identification Detector (PID) [25], consisting of a barrel of thin plastic scintillators surrounding the target, was used to identify charged particles.

Two different settings were used for the experiment. The E_γ = 200–310 MeV data were taken using a 1204 MeV electron beam with 1.5 mm diameter collimator. The E_γ = 320–450 MeV data used a 1508 MeV incident electron beam with the same collimation. To allow the largest photon flux in the polarised energy region, without incuring excessive dead-time in the read-out system, the tagger focal plane detectors (FPD), corresponding to $E_\gamma \leq 140$ MeV, were switched off. The fraction of tagged photons passing through the collimator ("tagging efficiency") was measured at a reduced beam current by moving a $\sim 100\%$ efficient lead glass detector into the photon beam. An ionisation chamber monitored the photon flux during the experiment.

A photon beam with strong linear polarisation can be produced using the technique of coherent bremsstrahlung [26,27] where the electron beam scatters coherently from a suitably aligned crystal radiator. A thin diamond crystal, with low mosaic structure, minimises the energy smearing of the coherent spectrum arising from electron multiple scattering effects and crystal defects in the lattice [28]. Collimation enhances the polarisation of coherent bremsstrahlung as well as defining the size of the photon beam. The inital alignment of the diamond was carried out using the Stonehenge technique [29]. By accurately orienting the diamond radiator with respect to the incident electron beam it is possible to arrange that one crystal reciprocal lattice vector (normally $[0\bar{2}\bar{2}]$) dominates the coherent photon production process. Fine tuning of the orientation allows the plane of linear polarisation to be set and the maximum polarisation to be tuned to a particular photon energy. Two orthogonal photon polarisation planes were used. These were set at azimuthal angles of $\pm 45^\circ$ with respect to the equatorial plane of the CB detector. Coherent bremsstrahlung is more strongly forward focussed than incoherent background. The tagging efficiency consequently varies strongly with E_γ. Tagging efficiency values of $\sim 40\%$ were obtained in the coherent peak at around 300 MeV.

An enhancement spectrum is obtained by dividing the E_γ spectrum from the diamond by that of an amorphous radiator, assuming the incoherent background is reasonably approximated by the amorphous radiator. The enhancement spectrum does not exhibit the $\sim 1/E_\gamma$ dependence of bremsstrahlung radiation and is not affected by channel-to-channel variations in the FPD efficiency. An analytical bremsstrahlung calculation, *AnB* [30], of the coherent bremsstrahlung spectrum provided a reasonably good description of the measured enhancement spectrum [31]. The *AnB* code accounts for thermal motion of atoms in the radiator and multiple scattering effects, and uses realistic values of parameters including beam energy, divergence, photon collimation and the properties of the diamond radiator. The small difference between the measured enhancement spectrum and the *AnB* calculation is used to make a slight improvement in the *AnB* calculation of the polarisation as described in ref. [32]. This improved prediction is used in fig. 1.

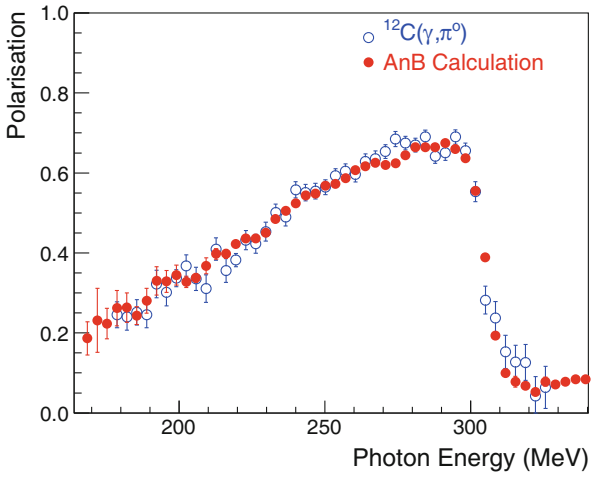

Fig. 1. Comparison of the photon polarisation obtained from the $^{12}\mathrm{C}(\vec{\gamma},\pi^0)$ reaction (blue open circles) and calculated using the *AnB* code, as discussed in the text (red solid circles).

An independent check of the photon polarisation for both photon energy settings was made by measuring the azimuthal asymmetry of the coherent $^{12}\mathrm{C}(\vec{\gamma},\pi^0)$ reaction. Since $\Sigma = -1$ for coherent π^0 photoproduction reactions from $J^\pi = 0^+$ nuclei [33], the observed asymmetry provides a direct measurement of the photon polarisation. Full details of this procedure are given in ref. [31]. Figure 1 shows the photon polarisation obtained using each method for the lower photon energy range E_γ = 200–310 MeV. The agreement between both methods is good and the *AnB* method was used in the data analysis. This comparison was used to provide an estimate of the systematic uncertainty in Σ arising from uncertainty in the photon polarisation. This is discussed further in sect. 5.

Graphite and polythene (CH_2) discs were used as targets for the present experiment. A 2.51 mm thick carbon disk was used for the lower photon energy setting, with a thicker (4.05 mm) disc used for the higher energies. A 5.97 mm polythene disc was used for the proton energy calibration using the $\mathrm{p}(\gamma,\pi^0)\mathrm{p}$ reaction. All the targets were mounted at an angle of 45° to the photon beam. This increases the effective target thickness while on average reducing the amount of material protons travel through before reaching the CB detector.

The CB is a highly segmented total energy electromagnetic calorimeter covering 94% of 4π sr. The 672 NaI crystals have a length of 40.6 cm which is sufficient to stop 425 MeV protons. The energy of each particle de-

tected in the CB is reconstructed from the total energy deposited in a cluster of adjacent crystals. Energy deposited by charged hadrons usually involves only a very small number of crystals. The direction of the particle is obtained from a weighted mean of the positions of the crystals that fire [31].

Charged hadrons are identified using their differential energy loss measured in the PID detector, together with the energy deposited in the CB. The PID also provided trigger timing information for events with at least one charged particle in the final state. It consists of 24 EJ204 scintillators arranged to form a 10 cm diameter barrel. Each of the scintillators is 31 cm long, 13 mm wide and 2 mm thick. The cross section of each element is a right-angled trapezium to minimise gaps between elements. Each element is wrapped separately in foil and the barrel is light-proofed. At one end of the PID, light guides couple each scintillator to its PMT. The cylindrical design of the PID around the target gives full 360° azimuthal coverage and the length of the scintillators ensured the polar angle coverage matched that of the CB.

The experimental trigger required the summed energy from all 672 elements in the CB to be more than 50 MeV and two or more clusters of CB detectors to register signals.

5 Data analysis

The photon asymmetry Σ has been determined as a function of E_γ, E_m, $\mathbf{P}_\mathrm{r}$ and the polar angles θ of the ejected protons. In the later stages of the analysis cuts on E_m and on the absolute difference in azimuthal angles ϕ of the two protons, $\alpha = |\phi_1 - \phi_2|$, have been applied.

The recoil momentum is obtained from the measured momenta of the photon $\mathbf{P}_\gamma$ and the two emitted nucleons,

$$\mathbf{P}_\mathrm{r} = \mathbf{P}_\gamma - \mathbf{P}_1 - \mathbf{P}_2. \quad (1)$$

The missing energy is determined from

$$E_\mathrm{m} = E_\gamma - T_1 - T_2 - T_\mathrm{r} = E_\mathrm{s} + E_\mathrm{x}, \quad (2)$$

where T_1, T_2 and T_r are the kinetic energies of the two outgoing nucleons and the residual system, respectively. E_s is the separation energy for two-nucleon emission (27 MeV for the reaction studied) and E_x is the excitation energy of the residual nucleus. The kinetic energy of the residual system is typically small and is accessed through P_r.

The timing of signals from the FPD was aligned using data from the tagging efficiency measurements. The timing of the (γ,pp) reaction was taken from the PID detector. The FPD-PID coincident timing peak had a FWHM of 2.3 ns. Subtraction of suitably normalised random event samples, obtained from regions away from the coincident peak, allowed the yield of the reaction to be determined.

The response of the CB to protons and photons was calibrated using data from the two-body reaction $\mathrm{p}(\gamma,\pi^0\mathrm{p})$ in which the π^0 was reconstructed from its $\pi^0 \to \gamma\gamma$ decay photons. Background reactions on C nuclei in the CH_2 target were removed by calculating the expected proton angle from the photon energy and the measured π^0 momentum and then only accepting events consistent with two-body kinematics. Scintillation signals were observed for a wide range of proton and photon energies and the gains of the NaI crystals were aligned. As protons and photons deposit their energy at different depths in the crystals, a proton energy-dependent correction factor [31] was derived to link the proton energy calibration to that established for photons.

Proton selection was made on the basis of ΔE-E plots constructed from the signals in the PID and CB. Proton and pion peaks were clearly identified in the pulse height spectrum from each PID element. The relative gain of each PID element was adjusted until the mean energy deposits for protons and pions corresponded to those predicted by a GEANT4 simulation. After gain matching both the PID and CB detectors a universal polygon cut was used to select protons in the ΔE-E plot for all PID elements. This method ensured that there was no bias introduced into the proton azimuthal yields. Events corresponding to the (γ,pp) reaction were obtained by requiring two, and only two, detected protons from these ΔE-E cuts.

The average energy losses of protons passing through target material and the detector elements depend strongly on their angles and energies. Energy-dependent corrections were calculated for protons detected in each CB element and stored in a look-up table [31]. In the analysis, the appropriate correction was extracted from this table and applied to each detected proton.

In the analysis of previous $^{12}\mathrm{C}(\gamma,2\mathrm{N})$ cross section data at $E_\gamma < 157$ MeV [34] the data were split into a number of missing energy regions. For the $^{12}\mathrm{C}(\gamma,\mathrm{pn})$ reaction, the region $E_\mathrm{m} < 40$ MeV has recoil momentum spectra that are well described by photon absorption on $(1\mathrm{p})^2$ nucleon pairs whereas for higher E_m, up to 70 MeV, the recoil momentum spectra are described by the emission of nucleon pairs from (1p)(1s) orbits. For the $^{12}\mathrm{C}(\gamma,\mathrm{pp})$ reaction the recoil momentum spectra were observed to be well described by photon absorption on $(1\mathrm{p})^2$ nucleon pairs at all missing energies up to 70 MeV. For the present data, cuts on missing energy of $E_\mathrm{m} < 40$ MeV and $40 < E_\mathrm{m} < 70$ MeV were applied in the later stages of the analysis to study any differences in Σ with E_m.

The proton energy resolution of the CB was measured to be ~ 25 MeV FWHM for protons from the $\mathrm{p}(\gamma,\mathrm{p}\pi^0)$ reaction [31], measured using a polythene target. The protons measured had similar average energies to those from the $^{12}\mathrm{C}(\gamma,\mathrm{pp})$ reaction and from this the (γ,pp) E_m resolution is estimated to be ~ 35 MeV. This is significantly larger than the resolution of the earlier work [34]. It is therefore expected that there will be considerable mixing between the two missing energy regions studied.

In the case where the photon is absorbed on a stationary nucleon pair the ejected nucleons and the incident photon are coplanar. However, the initial Fermi motion of the nucleons generally produces a pair momentum component perpendicular to the photon which causes the outgoing pair and the incident photon to be non-coplanar. In

selecting the appropriate azimuthal angle ϕ for the reaction we took a weighted average of the azimuthal angles of the two protons,

$$\phi = \frac{P_1(\sin\theta_1)\phi_1 + P_2(\sin\theta_2)(\phi_2 - \pi)}{P_1 \sin\theta_1 + P_2 \sin\theta_2}, \quad (3)$$

where $\theta_{1,2}$ and $\phi_{1,2}$ are the polar and azimuthal angles of the two protons. This weights the azimuthal angles of the two protons according to the component of their momentum perpendicular to the photon beam.

The photon asymmetries Σ were extracted using the equation

$$\frac{Y_\parallel - Y_\perp}{Y_\parallel + Y_\perp} = P\Sigma cos(2(\phi - \phi_0)), \quad (4)$$

where P is the photon polarisation, $Y_\parallel$ and $Y_\perp$ are the yields for data taken with two orthogonal photon polarisation orientations and ϕ_0 is the azimuthal angle of the perpendicular photon polarisation plane with respect to the vertical lab coordinate axis. The 2π azimuthal coverage of the CB allows data from all azimuthal angles to be used in the evaluation of Σ. Corrections were made [31] to take account of the small differences in photon yields (less than 1%), and in photon polarisation ($\sim 3\%$), between the two polarisation orientations. The offset azimuthal angle $\phi_0 = 46.8°$ was deliberately set well away from the lab horizontal plane where the CB has a thin dead region.

For Σ measurements systematic uncertainties in the location of detector systems, detector efficiencies, target density, etc., largely cancel leaving the photon polarisation P as the largest source of systematic uncertainty. As discussed in sect. 4, two different techniques of obtaining P were studied. In kinematic regions where both techniques could be used, the small observed differences in the extracted values of P resulted in differences of 0.02 or less in Σ. This value is taken as the systematic uncertainty arising from the photon polarisation.

Systematic uncertainties may arise due to particle misidentification, *e.g.*, from some charged pions falling within the proton cut. An estimate of this uncertainty was made by studying Σ with tighter cuts around the proton ridges observed in the ΔE-E plots. The effect was found to be small, affecting the magnitude of Σ by < 0.01.

A further systematic uncertainty may be introduced due to an incorrect identification of the azimuth of the reaction plane using eq. (3). A measure of the uncertainty from this source was estimated by analysing the data for $\alpha = 160$–$180°$ and 170–180°. In the latter case the two protons are more nearly coplanar and the azimuth of the reaction is better defined. The tighter cut increased the magnitude of Σ by ~ 0.01.

The systematic uncertainty in Σ from all of these effects is estimated to be no more than ± 0.03 for $E_\gamma < 320$ MeV and no more than ± 0.04 for $E_\gamma > 320$ MeV. As the systematic uncertainties are smaller than the statistical accuracy of most of the results, only the statistical uncertainties are plotted on the graphs in sect. 6.

Figure 2 shows the strong observed correlation between α and P_r for all E_m in the range $E_\gamma = 200$–310 MeV.

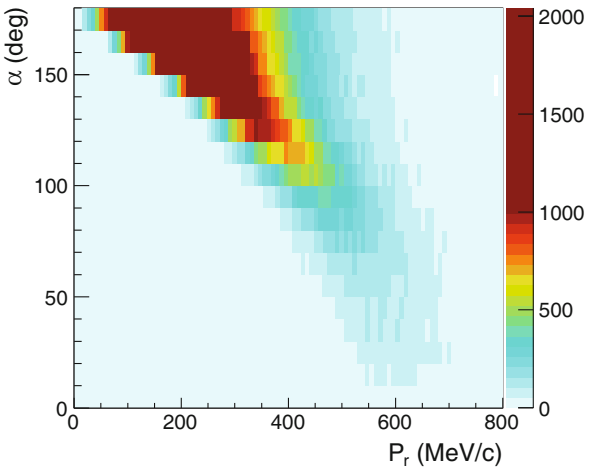

Fig. 2. Observed correlation between the angle $\alpha = |\phi_1 - \phi_2|$ and the recoil momentum P_r for all E_m and $E_\gamma = 200$–310 MeV.

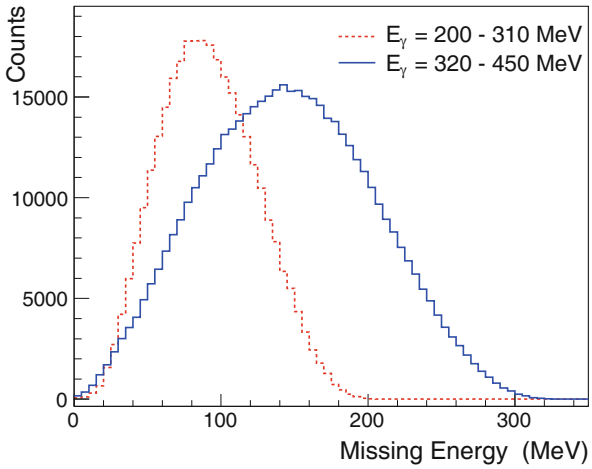

Fig. 3. ^{12}C(γ,pp) missing energy distributions for $E_\gamma = 200$–310 MeV (red dotted histogram) and $E_\gamma = 320$–450 MeV (solid blue histogram).

The (γ, pp) yield is largest in kinematics with large values of α. This region also corresponds to low values of P_r. Lower values of α may be a result of either increasing values of P_r, arising from Fermi motion of the nucleons, or the result of FSI. It is clear from the figure that the reaction strength drops off rapidly with increasing values of P_r. Making cuts on high values of α, or excluding large values of P_r, are both methods that can be expected to increase the relative contribution from direct 2N emission events and reduce the contribution from events that have undegone large FSI.

6 Results

6.1 Missing energy

The E_m distributions for ^{12}C(γ,pp), obtained by averaging data over all azimuthal angles, are shown in fig. 3 for

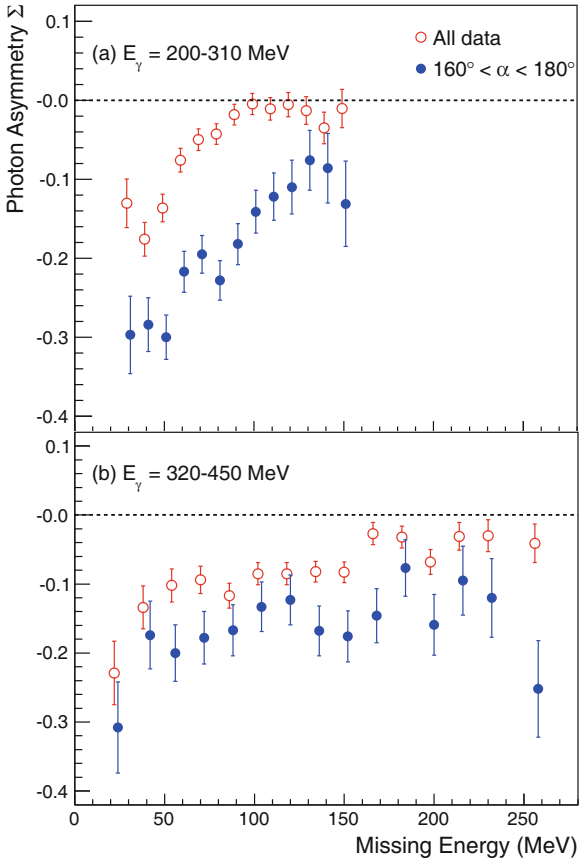

Fig. 4. Photon asymmetry Σ for ^{12}C($\vec{\gamma}$,pp) (open red circles) plotted as a function of missing energy E_m for (a) E_γ = 200–310 MeV and (b) E_γ = 320–450 MeV. Data with 160° < α < 180° are shown by solid blue circles. For clarity the blue data points are offset by +2 MeV.

both E_γ = 200–310 MeV and E_γ = 320–450 MeV. Both distributions rise smoothly from threshold as in previous measurements [16,5] at similar photon energies. The small shoulder at $E_m \sim 35$ MeV found at E_γ = 200–250 MeV in ref. [16] is not seen in the present work, possibly due to the poorer energy resolution. The low strength just above threshold indicates that the residual nucleus is not often left in or near its ground state. Most of the ^{12}C(γ,pp) yield is found at higher missing energies where much of the strength is thought to come from initial pion production, multi-nucleon knockout and mechanisms with FSI [5, 14]. At high E_m the spectra for both photon energy ranges fall off smoothly up to the limits determined by the useful energy range of the detectors.

The photon asymmetry Σ of the ^{12}C($\vec{\gamma}$,pp) reaction is shown in fig. 4 as a function of E_m. For E_γ = 200–310 MeV, there is a strong negative asymmetry at $E_m \sim$ 40 MeV. At higher E_m, Σ decreases in magnitude and above 100 MeV it is consistent with zero. As noted earlier, Valencia model calculations predict substantial contributions from complex two-step mechanisms in this missing energy region [14,35] and such complex processes may be expected to have small asymmetries.

For E_γ = 320–450 MeV (fig. 4(b)) the magnitude of the asymmetry just above the reaction threshold is greater than at lower photon energies and Σ retains an appreciable magnitude up to $E_m \sim$ 150 MeV. In this photon energy range there is expected to be a larger contribution from Δ currents [3].

As discussed in sect. 5, cuts on high values of α are expected to select events corresponding to direct 2N knockout and reduce contributions from FSI. Figure 4 also shows the E_m dependence of Σ for events with α = 160–180°. For the lower E_γ range, Σ is systematically increased for α = 160–180° compared to the uncut data, although the peak structure at low E_m is not so well defined. It is also larger on average for the higher E_γ range although the relative increase is smaller. For both E_γ ranges Σ has an appreciable magnitude up to the highest measured missing energies when these cuts are applied.

This analysis shows that the strongest asymmetries are observed when cuts are made to emphasise kinematics corresponding to direct two-nucleon knockout, and the magnitudes of Σ for direct two-proton emission are appreciable. It is observed that at high E_m, particularly for E_γ = 200–310 MeV, Σ is only appreciably different from zero when these cuts are applied.

6.2 Photon energy dependence of the asymmetry

The photon energy dependence of Σ is shown in fig. 5 for the same two missing energy regions, E_m < 40 MeV and 40 < E_m < 70 MeV, used previously [12]. It should be noted that the current E_m resolution is poorer than the earlier work and some mixing between the two E_m regions is expected. A cut on α = 160–180° has been applied to the data. This cut provides a broadly similar azimuthal acceptance as the earlier measurements of Powrie *et al.* [12] where the restriction was a result of the finite sizes of the detectors. However, the present data contain a wider range of proton polar angles.

The present measurements extend to higher E_γ values and have better statistical accuracy than those of Powrie *et al.* [12]. For E_m < 40 MeV there is reasonable agreement between the present measurement and previous work. Below E_γ = 240 MeV, Σ is relatively large at ~ -0.35. Both measurements show the magnitude of Σ drops to a low value around 260 MeV, before increasing again at higher E_γ. The reason for this feature is unclear although it may be related to the decreased M2 multipole strength which falls to zero in this energy region [36]. The increase in magnitude to ~ -0.4 at 300 MeV may indicate a change in the dominant reaction mechanism. MacGregor *et al.* [37] noted the important influence of processes involving intermediate Δ excitation to the ^{12}C(γ,pp) reaction in this E_γ region. Above 300 MeV the asymmetry magnitudes fall rapidly before rising again.

The Gent theoretical calculations [3] shown in fig. 5 were specifically carried out for comparison with the earlier PiPToF ^{12}C($\vec{\gamma}$,pp) data [12] and used a Monte Carlo technique to average over the acceptance of the PiPToF

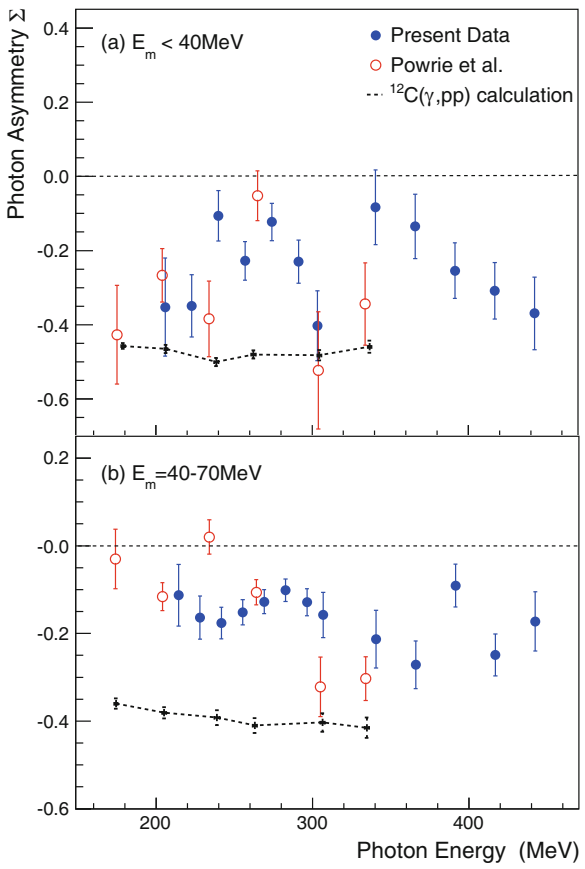

Fig. 5. Photon energy dependence of Σ for (a) $E_{\rm m} < 40$ MeV and (b) $40 < E_{\rm m} < 70$ MeV (solid blue circles). The red open circles are from Powrie *et al.* [12] and the black dashed lines are theoretical predictions from the Gent ^{12}C($\vec{\gamma}$,pp) direct knockout model [12] for (a) $(1p)^2$ pairs and (b) (1p)(1s) pairs.

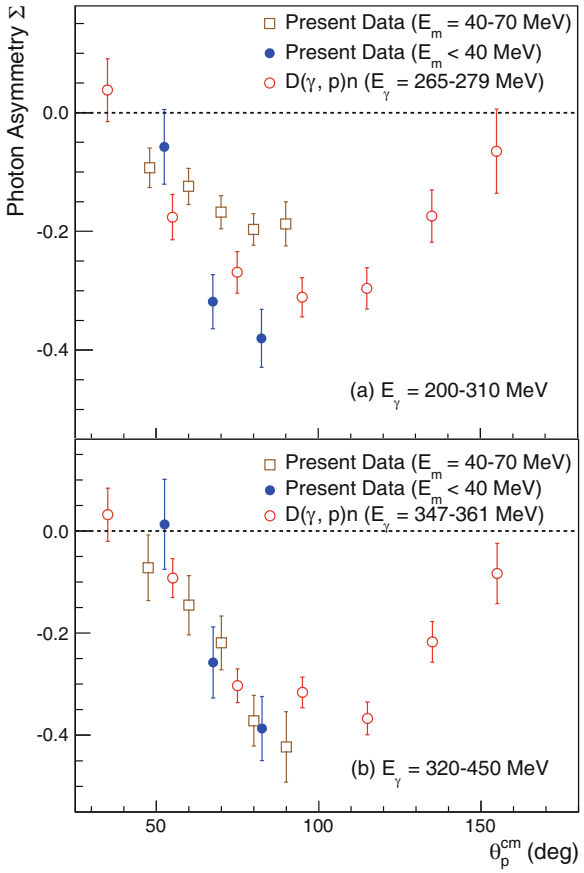

Fig. 6. Photon asymmetry Σ for ^{12}C($\vec{\gamma}$,pp) as a function of θ_p^{cm} for $E_{\rm m} < 40$ MeV (solid blue circles) and $E_{\rm m} = 40$–70 MeV (open brown squares) for a) $E_\gamma = 200$–310 MeV and b) $E_\gamma = 320$–450 MeV. Also shown is Σ for d($\vec{\gamma}$,p)n (open red circles) as a function of proton centre-of-mass polar angle for $E_\gamma = 265$–279 and $E_\gamma = 347$–361 MeV [39].

detectors. They include pion-in-flight and seagull MEC terms plus Δ currents. Calculations for low $E_{\rm m}$ are based on direct knockout of a $(1p_{3/2})$ pair and $(1p_{3/2})(1s_{1/2})$ knockout for higher $E_{\rm m}$. For (γ,pp) reactions, MEC are suppressed and only Δ currents and one-body terms contribute. The comparison between the calculations and the previous measurements suggested the magnitude of Σ predicted by the calculations was too large in the photon energy range $E_\gamma = 240$–290 MeV, although this comparison was hampered by the poor statistical accuracy of the earlier data. The present results have better statistical accuracy and confirm this difference. However, it would be instructive to compare the present data with more modern calculations extending to higher E_γ.

Figure 5(b) shows the photon energy dependence of Σ for $40 < E_{\rm m} < 70$ MeV. The current measurement shows much smoother variation with photon energy than the previous results of Powrie *et al.* [12]. The present results are smaller in magnitude around 320 MeV data and do not support a value close to zero at ~ 230 MeV. The Gent calculations significantly exceed the measured Σ at all photon energies in this missing energy region.

6.3 Angular dependence of the asymmetry

The measured ^{12}C(γ,pp) cross section has a distinct angular dependence [38] and theoretical calculations predict that Σ also has a strong angular variation [3]. For the first time, the angular dependence of Σ has been measured, which provides new information on this important observable.

Figure 6 shows measured Σ values for two E_γ ranges for $E_{\rm m} < 40$ MeV and $E_{\rm m} = 40$–70 MeV as a function of θ_p^{cm}, the polar angle of the ejected protons in the centre-of-mass frame of the photon and the protons in their initial state. To transform the proton angles into this reference frame their initial combined momentum was taken to be $-\mathbf{P}_{\rm r}$, which makes the assumption that the rest of the nucleus is a spectator and the effects of FSI and binding energy are negligible. In this reference frame the two protons are emitted with the same energy and back to back. As they are indistinguishable the results are presented in terms of the lower polar angle and hence extend only up to 90°. Again, some mixing between the two $E_{\rm m}$ regions is expected due to experimental resolution.

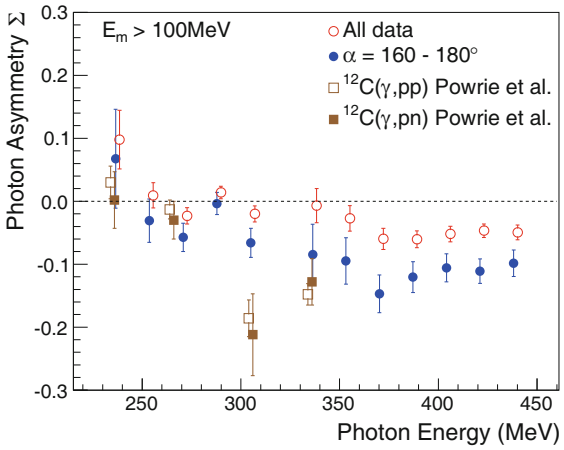

Fig. 7. Photon asymmetry Σ for ^{12}C($\vec{\gamma}$,pp) with (blue solid circles) and without (red open circles) angular cuts on α, as a function of E_γ, for $E_m > 100$ MeV, compared with ^{12}C($\vec{\gamma}$,pp) (brown open squares) and ^{12}C($\vec{\gamma}$,pn) (brown solid squares) data from Powrie *et al.* [12] with $E_m > 70$ MeV. The open red points are offset by 2 MeV for clarity.

For $E_m < 40$ MeV, in both E_γ ranges, Σ varies from around zero at 50° to ~ -0.4 near 90°. These observations are not inconsistent with the earlier measurements of the angular distributions of $\sigma_{\parallel}$ and $\sigma_{\perp}$ [18] at $E_\gamma = 290$–350 MeV, discussed in sect. 3, although a direct comparison is not possible.

Figure 6 also shows the measured angular distribution for Σ in the d($\vec{\gamma}$,p)n reaction [39] at similar photon energies to the present work. The deuterium data extend to angles greater than 90° as the proton and neutron from deuterium are distinguishable. For both E_γ ranges the angular distributions of the present ^{12}C($\vec{\gamma}$,pp) low E_m data are remarkably similar in both shape and magnitude to the deuterium data. The magnitude of Σ is slightly larger for ^{12}C($\vec{\gamma}$,pp) than for deuterium in the lower E_γ range. In the higher E_γ range the difference in magnitude is insignificant.

Angular distributions for $E_m = 40$–70 MeV are also shown in fig. 6. These Σ distributions have very similar shapes to those observed for $E_m < 40$ MeV. For $E_\gamma = 200$–310 MeV the magnitude is a factor of ~ 2 lower than the low E_m data. However, for $E_\gamma = 320$–450 MeV the magnitudes are very similar for both E_m ranges.

6.4 Photon asymmetries at $E_m > 100$ MeV

Comparisons of previously measured ^{12}C(γ,pp) E_m spectra [5,14] with predictions from the Valencia model [4] suggested that for $E_m > 70$ MeV direct two-proton emission makes a very small contribution. Above 100 MeV multistep processes contribute to the reaction cross section and for $E_\gamma < 250$ MeV photon absorption on a nucleon pair followed by FSI is thought to be the dominant process. Between 250 and 400 MeV 2N absorption plus FSI, 3N absorption and pion production with pion re-absorption in the nucleus all contribute. Above 400 MeV pion production with pion rescattering also contributes.

Figure 7 shows the E_γ dependence of Σ for $E_m > 100$ MeV, averaged over the total angular acceptance of the CB. The data with no angular cuts show no appreciable asymmetry below $E_\gamma = 350$ MeV, but have a small negative asymmetry at higher energies. These non-zero values at high E_γ indicate that at least some of the contributing processes have an intrinsic asymmetry, although Fermi motion and FSI effects would be expected to reduce the observed magnitude from that of the initial process. Cuts on the angle α, which select events where the two emitted nucleons and the incident photon are close to being co-planar, produce asymmetries with generally larger magnitudes. The values above 350 MeV are roughly doubled compared to the data with no angular cuts.

Comparisons are also made with previous ^{12}C($\vec{\gamma}$,pp) and ^{12}C($\vec{\gamma}$,pn) data [12], which measured Σ for $E_m > 70$ MeV up to $E_\gamma = 340$ MeV using the PiPTOF detector system. At high E_m both reaction channels are thought to have similar mechanisms [5]. Powrie *et al.* [12] suggested the substantial asymmetry values observed above 300 MeV may be due to pion production reactions followed by pion reabsorption. The initial pion production processes [40] are known to have a large negative asymmetry and their cross section becomes large at Δ-resonance energies.

7 Summary and conclusions

This work has provided new photon asymmetry data on the ^{12}C($\vec{\gamma}$,pp) reaction. The data have slightly poorer energy resolution than previous work [12], but have higher statistical accuracy. They extend to higher photon energies and present, for the first time, the angular dependence of Σ. The results agree reasonably well with previous measurements in regions of overlap.

It is observed that the ^{12}C($\vec{\gamma}$,pp) asymmetry has large negative values at $E_m \sim 40$ MeV where direct emission of nucleon pairs from $(1p)^2$ orbitals is expected. The asymmetry from the missing energy region $40 < E_m < 70$ MeV is also negative, but its magnitude is less than for lower missing energies.

It is demonstrated that kinematic cuts which select proton pairs with large values of α increase the magnitude of the observed Σ. These cuts are thought to enhance the relative yield of direct two-nucleon emission processes and discriminate against events that suffer large FSI.

Measurements of the E_γ dependence of Σ show that the asymmetry remains appreciable up to $E_\gamma \sim 450$ MeV, for both $E_m < 40$ MeV and $40 < E_m < 70$ MeV.

The angular distribution of Σ for $E_m < 40$ MeV is similar to that of the d(γ,p)n reaction in two polarised photon energy ranges $E_\gamma = 200$–310 MeV and $E_\gamma = 320$–450 MeV. The angular dependence for $40 < E_m < 70$ MeV has a similar shape in both photon energy regions. Its magnitude is similar for $E_\gamma = 320$–450 MeV, but lower by a factor ~ 2 for $E_\gamma = 200$–310 MeV. A more detailed interpretation of the present measurements will require improvements to currently available theoretical models.

The authors wish to acknowledge the outstanding support of the accelerator group and operators of MAMI. This work was supported by UK Science and Technology Facilities Council (STFC 57071/1, 50727/1), Deutsche Forschungsgemeinschaft (SFB 443, SFB/TR 16), DFG-RFBR, European Community-Research Infrastructure Activity (FP6), Schweizerischer Nationalfonds, US DOE and NSF, and Canadian NSERC.

References

1. C. Giusti, F.D. Pacati, M. Radici, Nucl. Phys. A **546**, 607 (1992).
2. S. Boffi, C. Giusti, F.D. Pacati, M. Radici, *Electromagnetic Response of Atomic Nuclei* (Oxford University Press, 1996) ISBN 0-19-851774-2.
3. J. Ryckebusch, D Debruyne, W. Van Nespen, Phys. Rev. C **57**, 1319 (1998).
4. R.C. Carrasco, E. Oset, Nucl. Phys. A **536**, 445 (1992).
5. T. Lamparter *et al.*, Z. Phys. A **355**, 1 (1996).
6. J. Ryckebusch *et al.*, Phys. Lett. B **291**, 213 (1992).
7. J. Ryckebusch *et al.*, Nucl. Phys. A **568**, 828 (1994).
8. C. Giusti, F.D. Pacati, Nucl. Phys. A **641**, 297 (1998).
9. C. Giusti, F.D. Pacati, Nucl. Phys. A **535**, 573 (1991).
10. D.J. Tedeschi *et al.*, Phys. Rev. Lett. **73**, 408 (1994).
11. F.V. Adamian *et al.*, J. Phys. G **17**, 1657 (1991).
12. C.J.Y. Powrie *et al.*, Phys. Rev. C **64**, 034602 (2001).
13. S. Franczuk *et al.*, Phys. Lett. B **450**, 332 (1999).
14. D.P. Watts *et al.*, Phys. Rev. C **62**, 014616 (2000).
15. G.E. Cross *et al.*, Nucl. Phys. A **593**, 463 (1995).
16. P.D. Harty *et al.*, Phys. Lett. B **380**, 247 (1996).
17. P.D. Harty *et al.*, Phys. Rev. C **57**, 123 (1998).
18. I.J.D. MacGregor, *Proceedings of the 5th Workshop on electromagnetically induced two hadron emission, Lund, 2001*, edited by P. Grabmayr *et al.* (2001) p. 314, `http://www.pit.physik.uni-tuebingen.de/grabmayr/CD-Lund2001/HTML/Contributions.html`, ISBN 91-631-1612-X.
19. K.-H. Kaiser *et al.*, Nucl. Instrum. Methods A **593**, 159 (2008).
20. A. Jankowiak, Eur. Phys. J. A **28**, s1.149 (2006).
21. J.C. McGeorge *et al.*, Eur. Phys. J. A **37**, 129 (2008).
22. I. Anthony *et al.*, Nucl. Instrum. Methods A **301**, 230 (1991).
23. S.J. Hall *et al.*, Nucl. Instrum. Methods A **368**, 698 (1996).
24. A. Starostin *et al.*, Phys. Rev. C **64**, 055205 (2001).
25. D. Watts, *in Calorimetry in Particle Physics, Proceedings of the 11th International Conference, Perugia, Italy 2004*, edited by C. Cecchi, P. Cenci, P. Lubrano, M. Pepe (World Scientific, Singapore, 2005) p. 560.
26. U. Timm, Fortschr. Phys. **17**, 765 (1969).
27. D. Lohmann *et al.*, Nucl. Instrum. Methods A **343**, 494 (1994).
28. J.D. Kellie *et al.*, Nucl. Instrum. Methods A **545**, 164 (2005).
29. K. Livingston, Nucl. Instrum. Methods A **603**, 205 (2009).
30. F.A. Natter *et al.*, Nucl. Instrum. Methods Res. B **211**, 465 (2003).
31. J. Robinson, *Two proton Knockout from Carbon using linearly polarised photons*, PhD thesis, University of Glasgow (2010).
32. D.I. Glazier *et al.*, Nucl. Instrum. Methods Res. A **664**, 132 (2012).
33. V. Bellini *et al.*, Nucl. Phys. A **646**, 55 (1999).
34. J.C. McGeorge *et al.*, Phys. Rev. C **51**, 1967 (1995).
35. L. Machenil *et al.*, Phys. Lett. B **316**, 17 (1993).
36. P. Wilhelm, J.A. Niskanen, H. Arenhövel, Nucl. Phys. A **597**, 613 (1996).
37. I.J.D. MacGregor *et al.*, Phys. Rev. Lett. **80**, 245 (1998).
38. T.T.H. Yau *et al.*, Eur. Phys. J. A **1**, 241 (1998).
39. S. Wartenberg *et al.*, Few-Body Sys. **26**, 213 (1999).
40. F.A. Berends, A. Donnachie, D.L. Weaver, Nucl. Phys. B **4**, 1 (1967).